A noninvasive rf probe for the study of ionization and dissociation processes in technological plasmas

V. J. Law[a] and A. J. Kenyon
Department of Electronic and Electrical Engineering, University College London, Torrington Place, London WC1E 7JE, United Kingdom

D. C. Clary
Department of Chemistry, Christopher Ingold Laboratories, University College London, Gordon Street, London WC1H OAJ, United Kingdom

I. Batty
Cambridge Analogue Technology, Ltd., 76 Rook Street, Cottenham, Cambridgeshire, CB4 8RB, United Kingdom

(Received 3 May 1999; accepted for publication 9 July 1999)

A swept frequency absorbance plasma diagnostic technique for measurement of self-resonance frequency, intrinsic plasma-tool distributed capacitance, radiative energy loss, and effective plasma capacitance is described. The *ex situ* probe measures the plasma properties independently of all contributions from the plasma-tool and transmission line connection to the rf supply. The technique employs a swept frequency source and a balanced equal ratio arm bridge to measure the frequency response of the plasma tool after the plasma has been extinguished under plasma conjugate matching conditions. The resonant frequency of the combination of capacitances due to plasma-tool geometry (intrinsic capacitance, C_i) and the matching network (C_m) exhibits a shift from the excitation frequency (13.56 MHz) that is dependent on the effective plasma capacitance. Resonance frequency shift data are given for He, Ne, Ar, O_2, N_2, and N_2O as a function of both pressure (0.02–0.8 mbar) and incident power (50 and 100 W). This technique allows the differentiation between dissociation and ionization processes within the plasma through a simple noninvasive rf measurement. [S0021-8979(99)03420-9]

I. INTRODUCTION

The aim of electrical characterization of plasma tools and technological plasmas is both to understand more fully the fundamental physical processes of dissociation and ionization within plasmas and to optimize real-time processes, batch-to-batch control, and to provide interactive control. The *ex situ* noninvasive diagnostic approach to characterization is, however, nontrivial, whether real-time or off-line. Off-line characterzation may be performed by measuring the conjugate position of the removed matching network with its input terminated with a 50 Ω resistor.[1,2] Real-time measurement using *ex situ* close-coupled (between the matching network and driven electrode) current loops and voltage probes,[3–5] dual-directional couplers,[6] filters,[7] and diplexer circuits,[8] all provide information at the fundamental frequency (f_0) or at integer multiples thereof. However, transferability of these techniques between plasma tools requires the external rf source to be immune to plasma-generated harmonics, tolerant of probe position phase error, and the establishment of open- and short-circuit calibration. Thus, before the electrical characterization of the plasma can be performed the plasma tool must be characterized in terms of radiative emission and network matching range with respect to the plasma process.

In this article an off-line swept frequency absorbance technique for the measurement of the self-resonance frequency (f_r), radiative losses, and intrinsic plasma-tool distributed capacitance (C_i) is described. The measurement apparatus is shown to be easily inserted at the 50 Ω impedance input of the plasma-tool matching network. In addition, the effective plasma capacitance (C_p) for a series of six gases (monatomic He, Ne, and Ar, diatomic O_2, N_2, and triatomic N_2O) are reported.

The measurement technique is based on the observation that a plasma excited at $f_0 = 13.56$ MHz within a parallel-plate plasma tool appears as capacitive susceptance across the intrinsic impedance of the plasma tool. As a result, the capacitance of the matching network (C_m) must be adjusted to compensate such that the total capacitance of the system (C_i plus C_m plus C_p) produces a resonance at 13.56 MHz. Historically, the plasma has been modeled as a linear LRC equivalent electrical circuit[1–5,7,9–11] or a nonlinear LRC-plus-diode equivalent electrical circuit.[12,13] For each model the electrical elements are distributed variously throughout the plasma volume to represent the three main plasma components: two dark space regions (plasma sheaths) and the plasma bulk. All components are connected in series and have a complex impedance of

$$Z_p = R_p \pm jX_p . \tag{1}$$

The reactance X_p represents the capacitance of the plasma sheaths; the resistor represents the real component of the plasma bulk and sheath losses. The real and imaginary components of the complex impedance vary according to the physical input parameters and mode of plasma production,

[a]Corresponding author; electronic mail: v.law@ee.ucl.ac.uk

i.e., volume, pressure, gas composition, rf power, and plasma-tool configuration. Extracting values for the effective plasma capacitance for different gases in a range of pressure and power regimes allows the study of chemical and physical processes within the bulk. Mechanisms such as electron attachment, ionization, and dissociation can be studied directly.

For a low pressure plasma containing a monatomic gas (He, Ne, or Ar: ionization potentials =24.6, 21.5, and 15.8 eV, respectively), the following observations can be made: plasma densities increase with the electron-neutral collision frequency and plasma capacitance increases with collapsing plasma-sheath thickness. The combined effect of these changes decreases both the real and the imaginary component of the complex impedance and increases plasma power dissipation.

Conversely, the extended electronic structure of polyatomic molecules, such as O_2, N_2, and N_2O, provide lower ionization potentials (12.2, 15.6, and 12.8 eV, respectively), and allow electron attachment dissociation pathways. The latter have marked energy thresholds (i.e., $e^- + O_2 = O + O^-$ at 4.3 eV and $e^- + N_2O = N_2 + O^-$ at 1.7 eV) and attachment coefficients that increase with increasing electric field and/or pressure.[14,15] The formation of these pressure-dependent products replaces the highly mobile electrons with much slower negative ions. The reduction in electron population leads to an increase in the real and a decrease in the imaginary component of the plasma complex impedance.

The above processes are modified by the dissipative nature of the plasma volume, rf modulation of ion species traversing the plasma sheath,[16] and ambipolar diffusion of charged species to the chamber walls.[17]

All the rf information to analyze the complex impedance of the plasma is contained in the plasma-tool matching network. The *L*-type-matching network used in most plasma tools is composed of a fixed series inductance, series capacitance (load), and shunt capacitance (tune) elements (see Fig. 2). The combined impedance of the elements protects the 50 Ω output stage of the rf generator and provides a high voltage to the plasma-tool open circuit prior to plasma ignition. In the presence of a plasma, the combined elements provide a complex conjugate match to the reactive load at the fundamental. Thus, at low pressure the susceptance of the shunt capacitance is at a maximum value and the series capacitance set at a value to counter the inductance of the transmission line. At increased pressure the capacitance of the shunt capacitor is reduced due to increased plasma capacitance while the series capacitance is adjusted to compensate for the increase in the real part of the complex impedance.

In the absence of a plasma the inevitable series inductance of the matching network and capacitance of the plasma-tool forms a series circuit across the transmission line and rf generator (where X_L increases with frequency and X_C decreases with frequency, and at the resonant frequency $X_L = X_C$).

To obtain a one-dimensional analysis of the plasma impedance, in terms of C_p, the following three resonance conditions must be satisfied:

$$f_r = \frac{1}{2\pi\sqrt{L_i C_i}}, \tag{2}$$

$$f_m = \frac{1}{2\pi\sqrt{L_i (C_i + C_m)}}, \tag{3}$$

$$f_0 = 13.56 \times 10^6 = \frac{1}{2\pi\sqrt{L_i (C_i + C_m + C_p)}}, \tag{4}$$

where L_i and C_i are, respectively, the intrinsic inductance and capacitance of the plasma-tool, C_m the capacitance of the matching network, C_p the plasma capacitance, f_r and f_m the resonant frequencies of the system in the absence of a plasma and the measured resonant frequency of the plasma tool plus matching network, respectively, and f_0 the frequency of the rf generator to which the system is matched in the presence of a plasma.

Thus, Eq. (2) describes the self-resonance frequency of the plasma tool, Eq. (3) describes the measured resonance frequency of the plasma-tool plus matching unit after a plasma has been extinguished under conjugate-match conditions, and Eq. (4) describes the rf generator fundamental drive frequency at which the plasma-tool resonates under matched plasma conditions. Equations (3) and (4) can therefore be used to obtain a value for the effective plasma capacitance, C_p. In this measurement any intrinsic plasma inductance is cancelled by the plasma capacitive reactance to produce C_p. If this was not the case a plasma could not be struck and maintained with a series inductor in the, *L*-type matching network.

The method for obtaining C_p presented here differs from that described by Logan, Mazza, and Davidse[1] and van Roosmaien,[2] in that the swept frequency absorbance technique measures the entire plasma-tool frequency response while looking into the plasma-tool through the matching network when the rf generator is removed. In this way all reactive elements (including discontinuities) of the total plasma tool are factored into the measurement of C_p. This work also differs from Miller, Anderson, and Splichal[7] in that no additional close-coupled filters and inductors are used. Thereby the measurement can be readily made on any plasma tool without extensive reengineering.

II. EXPERIMENT

A. Plasma tool

The capacitively coupled plasma tool used in this study is an Oxford Plasma Technology (OPT) PD80 parallel-plate plasma tool configured in the asymmetric parallel-plate plasma-enhanced chemical vapor deposition (PECVD) mode. In this mode the larger diameter (top) electrode is capacitive coupled to a manual variable *L*-type matching network via a 1.5 m, RG213, 50 Ω transmission line. The counter electrode is formed by the smaller diameter plate to produce a ground-to-capacitively coupled electrode area ratio of 4:1. The two electrodes are separated by a glass outer cylinder to provide a total chamber volume of 7 ℓ with a

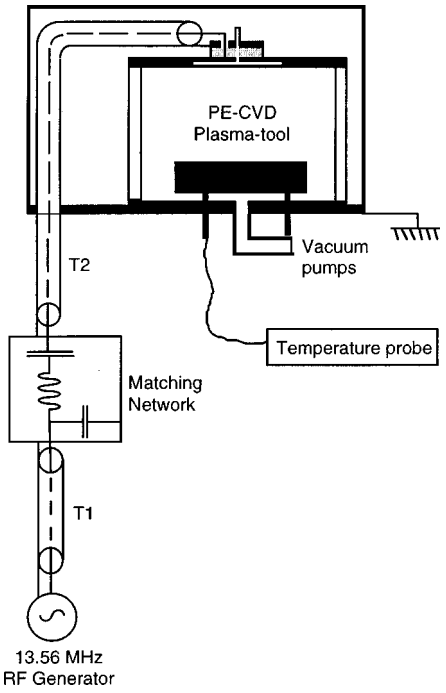

FIG. 1. A schematic representation of a PD80 capacitively coupled plasma-tool.

plate separation of 5 cm. The rf external circuit comprises a 13.56 MHz rf generator (ENI, HF-300) and an interconnecting 1.5 m, RG213, 50 Ω transmission line. The value of the intrinsic chamber capacitance (C_i) was calculated from the chamber physical geometry and C_t, the capacitance of the connecting transmission line ($C_i = C_c + C_t \sim 200$ pF), where $C_t = 100$ pF/m. The value of C_i was measured with an ISOTECH 9093 capacitance meter for both the intact (230 pF±5% @0.1 MHz) and open chamber configuration (210 pF±5%).[18] The difference between these values (20 pF) is principally due to the intact 5 cm electrode plate separation and dielectric chamber wall.

The purity of the gases used in the experiments was 99.99%. They were supplied to the plasma tool through 1/4 in. stainless steel tubes. The plasma-tool chamber was evacuated with a roots/rotary pump combination (240 $m^3 h^{-1}$). The chamber pressure was maintained by adjusting the gas flow rate and the effective pumping speed of the pumps. Electron attachment processes due to gas impurities for each series of measurements were minimized by evacuating the chamber for a minimum period of a day between each new gas experiment.

A schematic of the plasma tool is shown in Fig. 1. In Fig. 2 a general representation of the linear elements of the parallel-plate plasma tool is shown. The calculated phase delay and inductance at the excitation frequency of the individual fixed elements and known limits of the variable elements are listed in Table I.

B. Swept frequency measurement circuit

The circuit comprises a Hameg HM5006 combined tracking spectrum analyzer, and an equal ratio arm bridge with provision for a BALUN transformer[19] built by Cam-

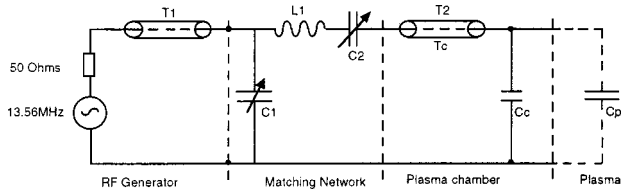

FIG. 2. A general representation of linear elements of the rf electrical circuit contained in the parallel-plate plasma-tool.

bridge Analogue Technology Ltd. The bridge has an open- and short-circuit error of ±1 dB between 10 and 200 MHz, and a directivity of 38 dB when used with a 50 Ω matched load at the reference port. A schematic representation of the complete circuit connected to the parallel-plate plasma tool is shown in Fig. 3.

The bridge is used to measure the return loss ratio (RLR (dB) $= 20 \log_{10} V_{\text{incident}}/V_{\text{reflected}}$) of the connected plasma tool with reference to a short-circuit termination at the bridge reference port. The bridge therefore measures the modulus of incident and reflected signals, but does not provide any phase information. The effective frequency range of the measurement is determined by the frequency position, the self-resonance frequency of the plasma-tool, and transmission line reflection due to its over extended electrical length.

The swept frequency measurement is performed off line after the plasma has been turned off with the variable elements of matching network unaltered from the complex conjugate position. To perform the swept frequency absorbance measurement correctly the following steps are followed.

Step 1. A plasma is established in the chamber and the matching network variable elements adjusted to produce a complex conjugate match. This procedure is monitored according to the incident and reflected power meter readings at the rf generator. The procedure is performed for 5 min to allow heating of the cables to stabilize. This step establishes the measurement of f_0.

Step 2. The plasma is extinguished by turning off the rf generator while keeping the position of the variable matching network elements fixed (N.B. for an auto-matching network the parking circuit for the variable elements must be turned off). Transmission line T_1 is now disconnected at the matching network and replaced directly with the bridge test port. It is important to note that the transmission line from the bridge to the plasma tool must be short. However, the transmission line from the bridge to the short circuit that defines the reference plane must be adjusted to provide a maximum return loss ratio when the initial measurement is

TABLE I. Calculated phase and reactance of fixed value individual elements at the fundamental and known limits of the matching network variable elements for the plasma-tool.

Plasma-tool	T_1 Phase delay (degrees)	C_1 (pF)	C_2 (pF)	L_1 (μH)	T_2 Phase delay (degrees)	Intact C_i (pF)
PD80	82	10–1000	10–500	2	40	230

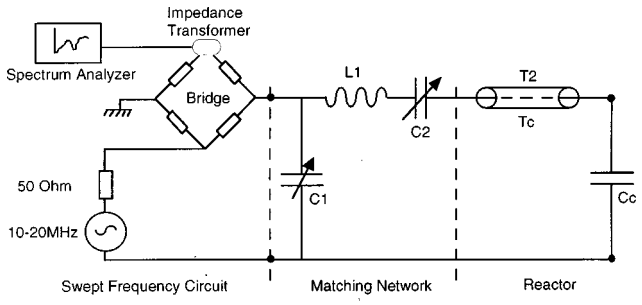

FIG. 3. A schematic representation of the swept frequency absorbance measurement circuit connected to the parallel-plate plasma-tool.

performed in step 3. The remaining bridge input and output ports are connected to the tracking generator and spectrum analyzer, respectively.

Step 3 establishes f_m and the return loss ratio. The swept frequency measurement of the plasma tool is performed, with the spectrum analyzer set to a frequency range of 10–20 MHz and a resolution bandwidth of 250 kHz. The return loss ratio is measured on the *y* axis of the spectrum analyzer as a function of swept frequency along the *x* axis. When the plasma tool resonates with the bridge, the reference termination is balanced with the plasma short circuit. This condition appears as an absorbance maximum (RLR_{max}, or minimum voltage standing wave ratio (*S*), where a value of 0 dB RLR =infinite *S*). For all experimental data reported here, the short-circuit reference plane was $l=2$ cm from the bridge.

III. RESULTS AND DISCUSSION

To illustrate the measurement technique, values of C_p for He, Ne, Ar, O_2, N_2, and N_2O plasmas have been obtained as a function of both incident power (50–100 W) and pressure (0.02–0.8 mbar). The gases were chosen to provide a range of monatomic and polyatomic gases with differing ionization potentials.

For clarity the experimental results are presented in three sections. Section A describes the self-resonance frequency for an empty chamber and the radiative losses of the plasma tool under Ar plasma conditions. Section B describes the swept frequency absorbance measurement for He, Ne, and Ar plasmas. Section C describes the experimental results for N_2, O_2, and N_2O plasmas.

A. Self-resonance frequency and radiative losses

With the matching network removed, the resonant frequency of the chamber and connecting transmission line T_2 was measured to be 19.2 MHz with a return loss ratio of -20 ± 1 dB and a 3 dB bandwidth of ~1.5 MHz. The result of this measurement is shown as a solid line in Fig. 4. From a knowledge of $C_i=230\,\text{pF}\pm5\%$, a series inductance value of $L_i\sim0.3\,\mu\text{H}\pm5\%$ is obtained from Eq. (2). Knowing that the plasma tool must resonate at the fundamental frequency of 13.56 MHz under plasma conditions with a capacitance of $C_m+C_p+C_i$, a capacitance versus frequency (f_m) calibration in terms of C_p can thus be obtained. This calibration is shown in Fig. 5.

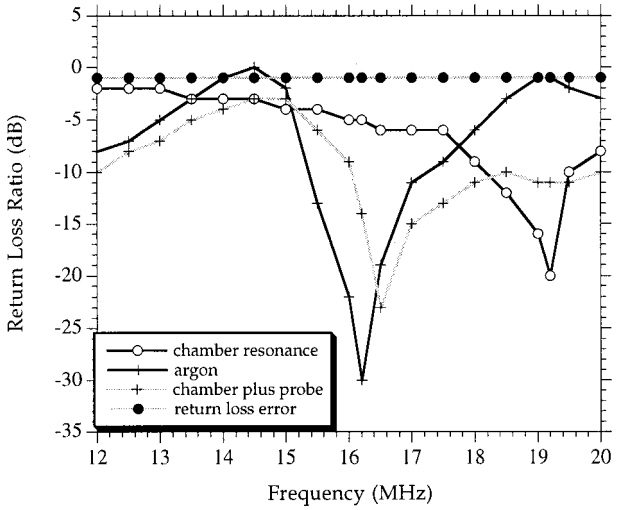

FIG. 4. Swept frequency absorbance measurement of plasma-tool self-resonance and measurement of f_m for a 50 W Ar plasma for both a clean electrode and with probes attached to the ground electrode.

A radiative energy loss measurement was performed on the plasma tool to ascertain the effect of the substrate heater and temperature measurement circuits used to maintain elevated temperatures of the grounded electrode during PECVD. A second indication of the radiative energy loss was obtained using a Marconi TF975 wavemeter placed at a fixed distance (0.5 m) from the plasma tool. The position of the attached probe is shown in Fig. 1.

The results of the two swept frequency absorbance measurements are shown in Fig. 4 for a 50 W Ar plasma at a chamber pressure of 0.05 mbar. It can be seen that the clean electrode data has an asymmetrical absorbance spectrum with a 3 dB bandwidth of 3.5 MHz centered at $f_m=16.2$ MHz (RLR$=-30\pm1$ dB). The absorbance asymmetry is characterized by the lower and upper frequency minimum RLR values (i.e., lower frequency limit=14.4 MHz, and upper frequency limit=18.8 MHz). For these conditions the

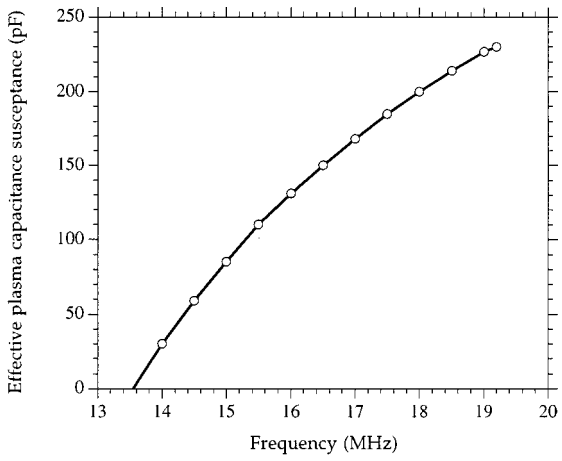

FIG. 5. Calibration of effective plasma capacitive susceptance (C_p) vs measured frequency (f_m).

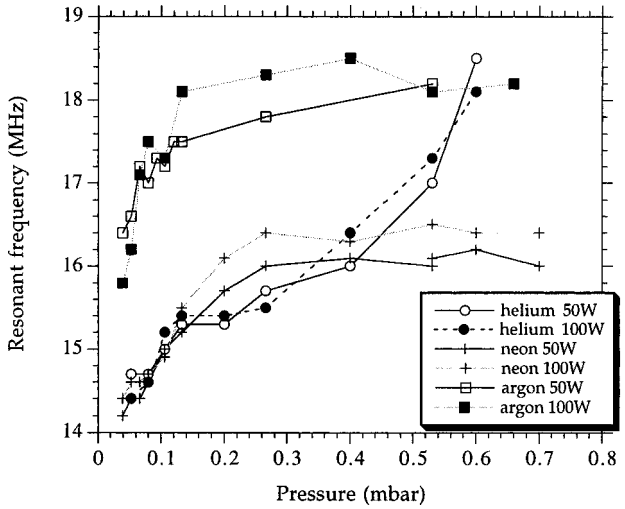

FIG. 6. Frequency response of matching network to 50 and 100 W He, Ne, and Ar plasmas as a function of pressure (mbar).

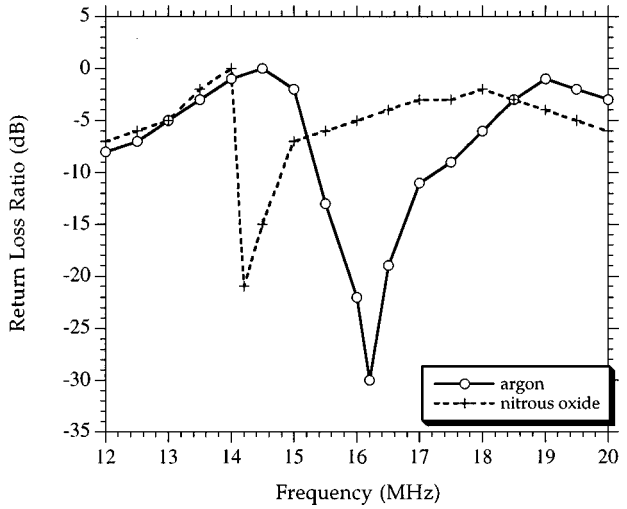

FIG. 7. Swept frequency measurement of 0.05 mbar Ar, and N_2O plasmas at an incident power of 50 W.

radiative energy loss as represented by the wavemeter detector current reading was in the region of 2–4 $\mu A\,cm^{-2}$.

The third curve in Fig. 4 represents the same Ar plasma condition with a heater controller and temperature probe attached. Under these false plasma matching conditions, f_m has now increased to 16.5 MHz (RLR$=-24\pm1$ dB), with the upper frequency maximum extended beyond 20 MHz at a RLR of -10 ± 1 dB. This extended absorbance region now defines the electromagnetic radiative energy loss from the plasma via the attached probes into free space. The radiative energy loss is confirmed by a wavemeter reading of 50 $\mu A\,cm^{-2}$. Under these conditions (or matching into a low impedance discontinuity) the minimum reflected power has a poor Q and is easily mistaken for the plasma conjugate position. This measurement illustrates the clinical use of the self-resonance absorbance measurement in defining the energy loss associated with the plasma-tool configuration and the need for careful rf design when close-coupled probes are used.

B. Monatomic He, Ne, and Ar

The plasma-tool frequency response to varying ion mass and ionization potential (He, Ne, and Ar) as a function of pressure (0.02–0.8 mbar) at incident powers of 50 and 100 W is reported in this section and shown in Fig. 6.

The values of f_m for the helium plasma are seen to increase linearly from 14.3 MHz ($C_p=20$ pF) to 18 MHz ($C_p=200$ pF) throughout the pressure range. The data spread suggests that there is no power dependency.

The neon plasma f_m curves exhibit similar low pressure behavior to the He plasma. Above 0.25 mbar the effective capacitance of the Ne plasma becomes a stable value of 16 MHz ($C_p=130$ pF). The results also indicate that there is no change in the dissipative nature of the Ne plasma between 50 and 100 W.

The argon plasma f_m data are seen to increase with pressure from 0.02 to 0.2 mbar, above which f_m levels to a value of ~18 MHz ($C_p=200$ pF). As with the neon data, there is no change in the dissipative nature of the argon plasma between 50 and 100 W.

The comparative capacitance data for these monatomic gases shows that C_p scales as the inverse of the gas ionization potential. At the lowest pressure (0.05 mbar) C_p increases from a value of 20 pF (which approximates the intact electrode separation capacitance). In the high pressure range (around 0.7 mbar) helium does not exhibit the same pressure dependency as neon and argon plasmas. The high pressure behavior is likely to be linked to the high ambipolar diffusion rate of helium (588 $cm^2\,s^{-1}$ Torr), which is four and eight times larger than neon and argon,[20] respectively.

The effective plasma capacitance data for argon is of the same order of magnitude as that reported by Roth,[18] Miller,[7] and Viera,[21] although Miller's capacitance data is higher by a factor of 4. This discrepancy is likely to be due to the difference in geometry of the two plasma tools (the reported GEC reference cell has two 10 cm diameter parallel-plate electrodes separated by 2.54 cm). We report the total capacitive contribution of the plasma without differentiation between the plasma sheaths. Our results, however, are in good agreement with Bushman, Edgar, and Trachtenberg who reported an effective capacitance of 200 pF for a 0.133 mbar (100 mTorr) CF_4H_2/Ar plasma in a Semi Group reactive ion etch system.

C. Diatomic O_2, N_2, and triatomic N_2O

In this section the plasma-tool frequency response to the chemical nature of nonpolar diatomic O_2 and N_2 and polar triatomic N_2O ($D=0.17$) is compared to monatomic argon. For these gases, low-energy dissociation/ionization and electron attachment dissociation are important fragmentation pathways.

In Fig. 7 the swept frequency absorbance measurements of 50 W Ar and N_2O plasmas at a fixed chamber pressure of 0.05 mbar are shown. The comparative data indicate that the

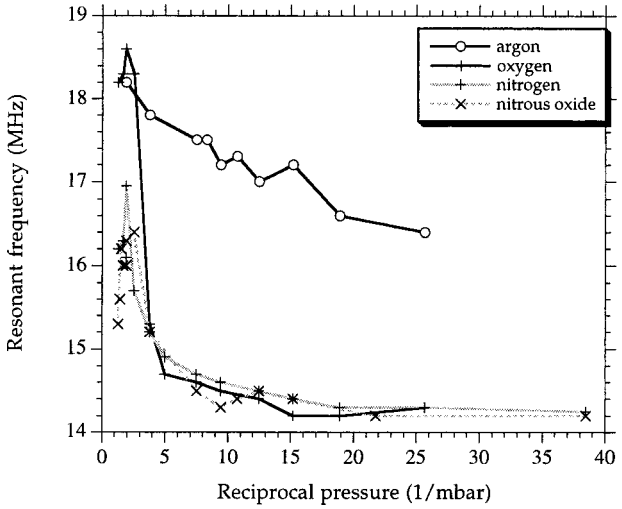

FIG. 8. Frequency response of matching network to 50 W Ar, O_2, N_2, and N_2O plasmas as a function of 1/pressure (1/mbar).

average f_m value for the N_2O plasma is some 2 MHz (effective capacitance=50 pF) lower than the Ar plasma.

A systematic investigation of f_m for O_2, N_2, and N_2O plasmas as a function of pressure (0.02–0.8 mbar) and incident rf power (50 and 100 W) has been performed. The result of these experiments are shown in Fig. 8 (50 W), and Fig. 9 (100 W). In each case f_m is plotted as a function of $1/P$ (1/mbar) to reveal its low pressure origin.

In Fig. 8, the f_m values for N_2, O_2, and N_2O plasmas are shown to have similar pressure dependencies, peaking at 0.5 mbar (2 $mbar^{-1}$). The magnitude of each peak is inversely proportional to ionization potential, with the N_2O plasma f_m value reaching the same value as that for the Ar plasma. Below 0.05 mbar all three plasmas reach an isotopic value of 14.3 MHz ($C_p=30$ pF), mirroring the helium and neon plasma data. At these low pressures the plasma sheath thickness is at a maximum and C_p approximates the intrinsic capacitance of the plasma-tool electrodes.

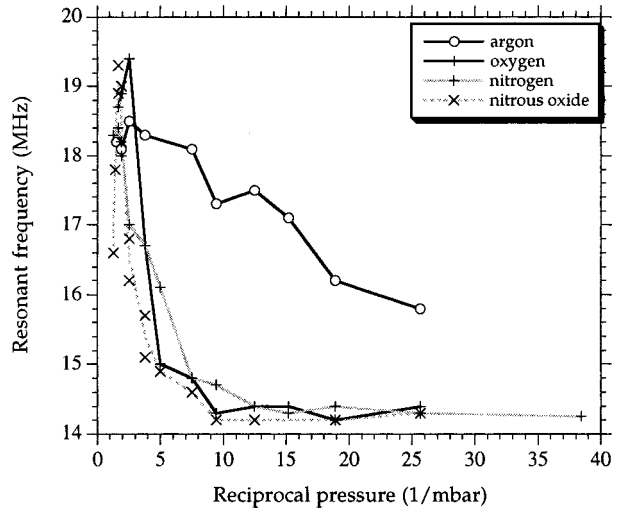

FIG. 9. Frequency response of matching network to 100 W Ar, O_2, N_2, and N_2O plasmas as a function of 1/pressure (1/mbar).

Nitrogen, oxygen, and N_2O plasmas have similar high pressure dependency at both 50 and 100 W. On increasing the power from 50 to 100 W the N_2O plasma capacitance increases from 18.5 to 19.5 MHz ($\Delta C_p=24$ pF), that for the N_2 plasma is increased from 16.5 to 18.5 MHz ($\Delta C_p=64$ pF) and that of the O_2 plasma from 17 to 19.5 MHz ($\Delta C_p=74$ pF).

The comparative capacitance data for the series of gases reported here indicate that for monatomic gases C_p scales with the inverse of the gas ion ionization potential, whereas for diatomic and polyatomic gases C_p is determined by the incident power. These results may be interpreted in terms of the increased availability of dissociation pathways for diatomic and polyatomic molecules.

IV. CONCLUSIONS

An *ex situ* off-line swept frequency absorbance measurement of a parallel-plate plasma tool has been described. The measurement technique factors in all the contributions from the plasma tool and the transmission line. The self-resonance frequency, radiative energy loss, and plasma-tool distributed intrinsic capacitance can be evaluated. The measurement technique allows for electromagnetic compatibility precompliance testing of the plasma tool, plus modification of the matching network and chamber to a specific process gas which is characterized by its effective plasma capacitance. The results also show that plasma tools intended for a wide range of processes should be tested with gases of different ionization potential, mass, and electronegativity across a pressure range from the lowest possible strike pressure to at least 0.5 mbar to ensure adequate range in the matching network. The technique is also useful for detecting ''false matches'' in which a minimum in reflected power at the matching network is due to transmission line reflections rather than a consequence of optimum power transfer to the plasma.

ACKNOWLEDGMENTS

The authors are grateful to Dr. Nina Thornhill at UCL, and Mike Cooke of OPT for helpful discussions regarding applications of the technique.

[1] J. S. Logan, N. M. Mazza, and P. D. Davidse, J. Vac. Sci. Technol. **6**, 120 (1969).
[2] A. J. van Roosmaien, J. Appl. Phys. **42**, 416 (1983); A. J. van Roosmaien, W. G. M. van den Hoek, and H. Kalter, *ibid.* **58**, 653 (1985).
[3] M. A. Sobolewski, J. Vac. Sci. Technol. A **10**, 3550 (1992); M. A. Sobolewski, J. Res. Natl. Inst. Stand. Technol. **100**, 341 (1995).
[4] S. Bushman, T. F. Edgar, and I. Trachtenberg, J. Electrochem. Soc. **144**, 721 (1997); N. StJ. Braithwaite, Plasma Sources Sci. Technol. **6**, 133 (1997).
[5] P. J. Hargis *et al.*, Rev. Sci. Instrum. **65**, 140 (1994).
[6] C. Garvin, D. Grimard, J. W. Grizzle, and B. E. Gilchrist, J. Vac. Sci. Technol. A **16**, 595 (1998); H. M. Park, C. Garin, and J. W. Grizzle, J. Electrochem. Soc. **145**, 4247 (1998).
[7] P. A. Miller, H. Anderson, and M. P. Splichal, J. Appl. Phys. **71**, 1171 (1998); P. A. Miller, L. A. Romero, and P. D. Pochan, Phys. Rev. Lett. **71**, 863 (1993).
[8] I. Batty, M. Cooke, and V. J. Law, Vacuum **52**, 509 (1999).
[9] J. W. Butterbaugh, L. D. Baston, and H. H. Sawin, J. Vac. Sci. Technol. A **8**, 916 (1990).

[10] E. Gogolides, J-P. Nicolai, and H. H. Sawin, J. Vac. Sci. Technol. A **7**, 1001 (1989).
[11] B. M. Annaratone, V. P. T. Ku, and J. E. Allen, J. Appl. Phys. **77**, 5455 (1995).
[12] C. M. Horwitz, J. Vac. Sci. Technol. A **1**, 60 (1983).
[13] M. Ardehali and H. Matsumoto, Jpn. J. Appl. Phys., Part 1 **32**, 3029 (1993).
[14] D. S. Burch and R. Geballe, Phys. Rev. **106**, 183 (1957).
[15] N. E. Bradbury and H. E. Tatel, J. Chem. Phys. **2**, 835 (1934).
[16] J. W. Coburn and E. Kay, J. Appl. Phys. **43**, 4965 (1972).
[17] V. J. Law, Vacuum **51**, 463 (1998).
[18] W. C. Roth, R. N. Carlile, and J. F. O'Hanlon, J. Vac. Sci. Technol. A **15**, 2930 (1997).
[19] *Reference Data for Engineer: Radio, Electronics, Computer and Communications*, edited by E. C. Jordan, 7th ed. (H. W. Sams, Indiannapolis, 1968), pp. 12.33–35.
[20] *Basic Data of Plasma Physics*, edited by S. C. Brown (AIP, New York, 1994), pp. 1–26.
[21] G. Viera, J. Costa, F. J. Compte, E Gracia-Sanz, J. L. Andujar, and E. Bertran, Vacuum **53**, 1 (1999).